

Wilson Loops of Klebanov-Strassler like Wrapped Brane Models

Michael Warschawski ¹

*Department of Physics, Swansea University
Singleton Park, Swansea SA2 8PP, United Kingdom.*

Abstract

We describe the behaviour of the Wilson loops for a novel class of solutions developed in [1]. Phase transitions could be found for all source profiles discussed. This study has yielded a previously unknown peculiarity not yet seen, where a solution with $h_1 \approx h_{1c}$ a profile for which $\lim_{\rho \rightarrow \infty} S(\rho) = 1$ can develop a phase transition like behaviour. Furthermore, the possibility to create systems with several phase transition has been discussed in detail with positive results.

arXiv:1212.3472v1 [hep-th] 14 Dec 2012

¹pymw@swan.ac.uk

Contents

1	Introduction	2
2	General Theory	2
3	Towards the background	3
3.1	Flavorless Wrapped-D5	4
3.2	U-Duality	5
3.3	Flavor branes	6
3.4	Sigmoid-like profiles	7
3.5	Bump-like profiles	8
4	Phase Transition	9
4.1	Introducing ρ_*	10
4.2	Powers of tanh and x	12
4.3	Different profiles	12
4.4	A curiosity	14
5	Double phase transition	14
5.1	Double Bump and Tumbling profiles	15
5.2	Plateau profiles	17
6	Conclusions	18

1 Introduction

The *AdS/CFT* correspondence [2] links a large N d -dimensional conformal field theory to a quantum theory in AdS_{d+1} . More specifically, local operators of the conformal field theory are related to fields of the dual quantum gravity theory [3].

However, *AdS/CFT* and the more general gauge-gravity theories can be used to study non-local operators as well. One of the most interesting of such operators is the Wilson loop [4]. It is accessible from the string theory side, which is computationally significant and physically, it provides a basis for gauge invariant gluonic operators.

But even more important here, the potential of a quark-antiquark pair can be related to the VEV of a rectangular Wilson loop, whose side are equal to the $q\bar{q}$ separation and $T \rightarrow \infty$. In the gauge theory the Wilson loop $W(\mathcal{C})$ along a curve \mathcal{C} is defined as

$$W(\mathcal{C}) \equiv \frac{1}{N_c} \text{Tr} \{ P[e^{i \oint_{\mathcal{C}} A_\mu dx^\mu}] \}. \quad (1)$$

where N_c is the number of colors, P represents the path ordering of the exponential and A_μ are the gauge fields. In this paper we will assume the gauge fields to be in the fundamental representation, however higher order representations are feasible [6]. On the string side of the correspondence we have [5, 7]

$$\langle W(\mathcal{C}) \rangle = \int_{\partial F(\mathcal{C})} \mathcal{D}F e^{-S[F]} \quad (2)$$

where F is used to denote all fields of the string theory and ∂F their boundary values along \mathcal{C} .

We can approximate (2) using the steepest descent method. Here, the surface spanned by the strings ending on \mathcal{C} and obeying the Nambu-Goto action $S_{NG}(F)$, is minimised. Now, that we have approximated the VEV of the Wilson loop and we know that we can relate the qq potential to this VEV by $\langle W(\mathcal{C}) \rangle \approx e^{-ET}$ we see that

$$E_{qq} \approx \frac{S_{NG}}{T} \quad (3)$$

Convinced of the importance of Wilson loops, we will compute its properties for backgrounds proposed in [1], deepening our understanding of those solutions. These sets of solutions, are very interesting as they relate two very fruitful extensions of the original *AdS/CFT* correspondence. One of the extension is referred to as Klebanov-Strassler (KS) Models [16]. Here, a deformation is introduced that corresponds to an imbalance in the gauge groups of the field theory side of the correspondence. This puts the field theory in the mesonic branch [28, 29].

The other extension is usually referred to as wrapped brane models [11, 12]. Here, we obtain the field theory through a higher dimensional field theory on which we perform a Kaluza-Klein compactification with twisting.

Our solution are KS like as they share the same IR and UV behaviour, and nontrivially relate to wrapped-brane models as they can be constructed from such a model by the addition of N_f sources and applying U-Duality, a solution generating technique introduced in [8].

2 General Theory

Here, I will discuss how to compute Wilson loops, as well as the potential energy of the qq -pair using the ideas from above for holographic theories. The following is based on [15]. Consider a 10d spacetime:

$$ds^2 = -g_{\mu\mu}(\rho)(dx^\mu)^2 + g_{\rho\rho}(\rho)(d\rho)^2 + g_{\theta\psi}(\rho)dx^\theta dx^\psi \quad (4)$$

as well as the Nambu-Goto Action

$$S_{NG} = \int d\sigma d\tau \sqrt{\det[\partial_\alpha x^\mu \partial_\beta x^\nu G_{\mu\nu}]} \quad (5)$$

Now using the string gauge $\tau = t$ and $\sigma = x$ and not allowing the string to explore then internal space, we can transform (5) to

$$S_{NG} = T \int dx \sqrt{f^2(\rho(x)) + g^2(\rho(x))(\partial_x \rho)^2} \quad (6)$$

Where

$$f^2(\rho(x)) = g_{tt}g_{xx} \quad g^2(\rho(x)) = g_{tt}g_{\rho\rho} \quad (7)$$

Now, one can either solve the Euler-Lagrange equations of this system or transfer to the Hamiltonian picture and note that the Hamiltonian in the x direction is a constant of motion as the Lagrangian is independent of t . Either way, one will derive the following equation of motion for the string:

$$\frac{d\rho}{dx} = \pm \frac{f(\rho)}{g(\rho)} \frac{\sqrt{f^2(\rho) - f^2(\rho_0)}}{f(\rho_0)} \quad (8)$$

From here one can calculate that the length L of the static string configuration connecting two quarks is

$$L = \int dx = 2 \int_{\rho_0}^{\infty} \frac{g(\rho)}{f(\rho)} \frac{f(\rho_0)}{\sqrt{f^2(\rho) - f^2(\rho_0)}} d\rho \quad (9)$$

Now that we have all the ingredients we need, we can use equation (3) to obtain $E(L)$, the potential energy of the quark-antiquark pair as a function of their separation. This result is generally divergent, as we have to assume infinite quark masses in order to make the qq-pair static, which in turn allows us to obtain the rectangular Wilson loops needed. The infinite potential energy can be renormalized by subtracting the mass of the quarks $m_q = \int_0^\infty g(\rho) d\rho$. The renormalized result is

$$E = f(\rho_0)L + 2 \int_{\rho_0}^{\infty} \frac{g(\rho)}{f(\rho)} (\sqrt{f^2(\rho) - f^2(\rho_0)} - f(\rho)) d\rho - 2 \int_0^{\rho_0} g(\rho) d\rho \quad (10)$$

Now, the backgrounds [1] we will focus on might only be related to wrapped brane models in the technical sense discussed in the introduction, but due the fact that wrapped brane models are relatively simple to study, we will sketch the construction of our solutions of interest on their basis. We start from a generic wrapped brane model, modify it by applying the solution generating technique referred to as U-Duality or rotation and add N_f sources. First, these sources are introduced naively, but then will be distributed according to profiles that become increasingly complex in order to correct more and more unphysical behaviours that will be discussed more detailed later. At every stage we will evaluate equations (9) and (10) to illustrate the behaviour of Wilson loops discussed. Afterwards we will construct cases, where the change of $E(L)$ to linear behaviour is started off by a phase transition. This is then generalised to obtain solutions that produce several phase transitions.

3 Towards the background

The wrapped brane models consist of a metric ds^2 , a dilaton Φ and an RR-three form F_3 . To write down the background, we use $SU(2)$ left-invariant one-forms

$$\tilde{\omega}_1 = \cos \psi d\tilde{\theta} + \sin \psi \sin \tilde{\theta} d\tilde{\varphi}, \quad \tilde{\omega}_2 = -\sin \psi d\tilde{\theta} + \cos \psi \sin \tilde{\theta} d\tilde{\varphi}, \quad \tilde{\omega}_3 = d\psi + \cos \tilde{\theta} d\tilde{\varphi}, \quad (11)$$

and the vielbeins

$$E^{x^i} = e^{\frac{\Phi}{4}} dx^i, \quad E^\rho = e^{\frac{\Phi}{4}+k} d\rho, \quad E^\theta = e^{\frac{\Phi}{4}+h} d\theta, \quad E^\varphi = e^{\frac{\Phi}{4}+h} \sin \theta d\varphi, \quad (12)$$

$$E^1 = \frac{1}{2} e^{\frac{\Phi}{4}+g} (\tilde{\omega}_1 + a d\theta), \quad E^2 = \frac{1}{2} e^{\frac{\Phi}{4}+g} (\tilde{\omega}_2 - a \sin \theta d\varphi), \quad E^3 = \frac{1}{2} e^{\frac{\Phi}{4}+k} (\tilde{\omega}_3 + \cos \theta d\varphi). \quad (13)$$

Thus, in the Einstein frame, we have

$$ds_E^2 = \sum_{i=1}^{10} (E^i)^2, \quad (14)$$

$$F_3 = e^{-\frac{3}{4}\Phi} \left(f_1 E^{123} + f_2 E^{\theta\varphi 3} + f_3 (E^{\theta 23} + E^{\varphi 13}) + f_4 (E^{\rho 1\theta} + E^{\rho\varphi 2}) \right),$$

where we defined

$$E^{ijk..l} = E^i \wedge E^j \wedge E^k \wedge \dots \wedge E^l, \quad (15)$$

$$f_1 = -2N_c e^{-k-2g}, \quad f_2 = \frac{N_c}{2} e^{-k-2h} (a^2 - 2ab + 1),$$

$$f_3 = N_c e^{-k-h-g} (a - b), \quad f_4 = \frac{N_c}{2} e^{-k-h-g} b'.$$

3.1 Flavorless Wrapped-D5

To connect to Section 2, we have to move from the Einstein frame to the string frame. The metric can be obtained by multiplying ds_E^2 by $e^{\frac{\Phi}{2}}$. The metric elements relevant for the Wilson loop computation become

$$g_{tt} = e^{\Phi(\rho)} \quad g_{xx} = e^{\Phi(\rho)} \quad g_{\rho\rho} = e^{\Phi(\rho)+2k(\rho)} \quad (16)$$

There are 6 functions in the background (a, b, Φ, g, h, k) which depend on the radial coordinate ρ . The background is determined by solving the equations of motion for these functions. A system of BPS equations can be derived[9, 17, 18]. These equations show that all background functions can be expressed in terms of $Q(\rho)$ and $P(\rho)$, where

$$Q(\rho) = N_c (2\rho \coth(2\rho) - 1) \quad (17)$$

and P is a solution to the following differential equation

$$P'' + P' \left(\frac{P' + Q'}{P - Q} + \frac{P' - Q'}{P + Q} - 4 \coth(2\rho) \right) = 0 \quad (18)$$

(18) is usually referred to as the master equation. The background functions of interest to us are

$$e^{2k} = \frac{P'}{2} \quad e^{4\Phi-4\Phi_0} = \frac{2 \sinh(2r)^2}{(P^2 - Q^2)P'} \quad (19)$$

Interesting solutions can be found semi analytically by numerically connecting the large ρ expansion

$$P = e^{4\rho/3} \left[c_+ + \frac{e^{-8\rho/3} N_c^2}{c_+} \left(4\rho^2 - 4\rho + \frac{13}{4} \right) + e^{-4\rho} \left(c_- - \frac{8c_+}{3} \rho \right) + \frac{N_c^4 e^{-16\rho/3}}{c_+^3} \left(\frac{18567}{512} + \frac{2781}{32} \rho + \frac{27}{4} \rho^2 + 36\rho^3 \right) + \mathcal{O}(e^{-20\rho/3}) \right] \quad (20)$$

with the IR expansion

$$P = h_1 \rho + \frac{4h_1}{15} \left(1 - \frac{4N_c^2}{h_1^2}\right) \rho^3 + \frac{16h_1}{525} \left(1 - \frac{4N_c^2}{3h_1^2} - \frac{32N_c^4}{3h_1^4}\right) \rho^5 + \mathcal{O}(\rho^7), \quad (21)$$

We solve the master equation numerically, using (21) and its derivative as initial conditions. We then obtain the background functions using the relations (19). We then solve the Nambu-Goto Action, as outlined in Section 2 to obtain $L(\rho_0)$ and $E(\rho_0)$ given by (9) and (10). These two functions can be combined to give us $E(L)$. In this case, this leads to the following plots:

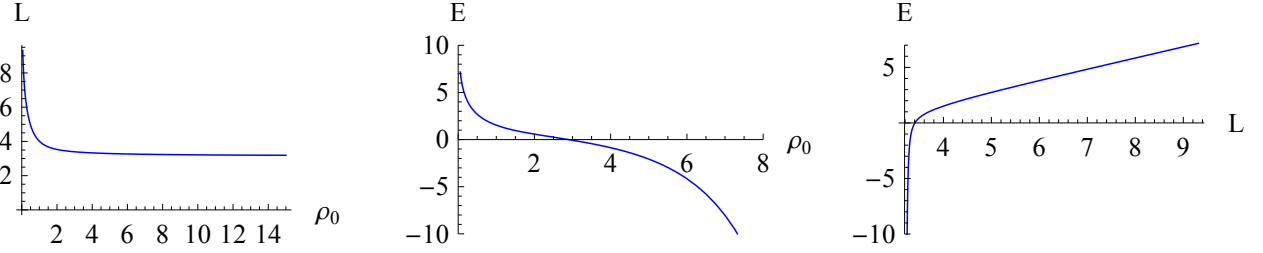


Figure 1: We used $N_c = 1$, $\Phi_0 = 0$ and $h_1 = 2$

As we can see on the left-hand diagram, there is a minimum, non-zero separation length beyond which the quarks do not want to be squished together. This gives the field theory a characteristic length scale. In other words, the theory has a UV cutoff beyond which we need a non-trivial UV completion. This has already been known in [19], which describes the existence of an irrelevant dimension 8 operator, which causes the UV of the theory to be not well defined. As one can see, for L close to its minimum value, E behaves Coulomb-like, but then grows linear for large L , showing that we deal with a confining theory.

3.2 U-Duality

So in order to make the connection with Klebanov-Strassler theories, a U-duality as it is described in [8] has to be applied to the system. This procedure is commonly referred to as rotation. It is a solution generating technique that schematically unites the backgrounds, by taking a solution to our master equation and mapping it to another background where new fluxes are turned on. While neither the background functions, nor Q and P change, the metric does and new fluxes are turned on. the metric elements relevant to our calculations are

$$g_{tt} = \frac{e^{\Phi(\rho)}}{\sqrt{\hat{h}}} \quad g_{xx} = \frac{e^{\Phi(\rho)}}{\sqrt{\hat{h}}} \quad g_{\rho\rho} = e^{\Phi(\rho)+2k(\rho)} \sqrt{\hat{h}} \quad (22)$$

where $\hat{h} = 1 - \kappa^2 e^{2\Phi}$ and κ can be chosen to be $\kappa = e^{-\Phi(\infty)}$, see [20]. The corresponding Wilson loop calculations give a very similar picture to the unrotated case. As in the last subsection, we still use $N_c = 1$ and $\Phi_0 = 0$ in the numerical calculations, but $h_1 = 3$ as $h_1 = 2$ gives a linear P and unbounded $\Phi(\rho)$, a solution to which rotation cannot be applied.

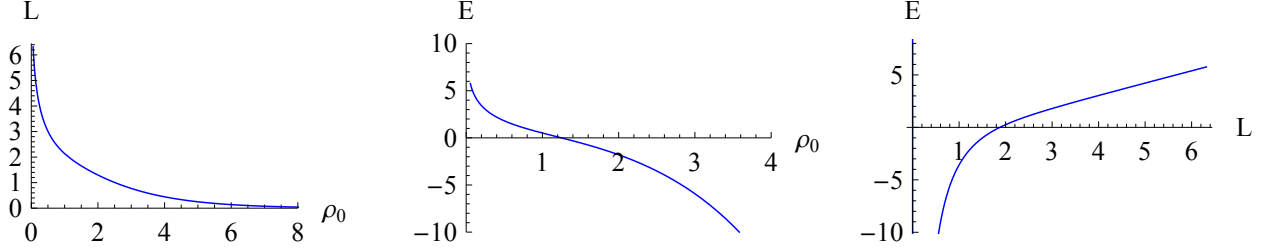


Figure 2: The rotated case. The rotation achieved the UV completion needed, which can be seen here as $\lim_{\rho_0 \rightarrow \infty} L = 0$

Evidently different to the last subsection, when we study a solution of P that does not remain linear in the IR, but rather grows exponentially $L(\rho_0) \rightarrow 0$ when $\rho_0 \rightarrow \infty$.

The analysis in this subsection has been very similar to [19]. However, in that paper, solutions to the master equation (18) have been studied, for which it was assumed that $P \gg Q$. This leads to an IR behaviour of P that is constant to first order and not linear [30]. This has led to some interesting effects like phase transitions. For our IR expansion (21) we have not been able to find any phase transitions. But in our case, no cusps in the string configuration that would break down the steepest descent approximation have been observed either.

3.3 Flavor branes

First we add sources in the original, naive way as described in [9, 10], without any kind of profile describing the distribution of the N_f branes. This time the form of the metric remains unchanged, while the background functions follow different equations. See [20, 21, 22, 9] for reference. Q and P are now given by

$$P'' + (P' + N_f) \left[\frac{P' + Q' + 2N_f}{P - Q} + \frac{P' - Q' + 2N_f}{P + Q} - 4 \coth(2\rho) \right] = 0, \\ Q(\rho) = \frac{2N_c - N_f}{2} (2\rho \coth(2\rho) - 1) \quad (23)$$

We now have for our background functions

$$e^{2k} = \frac{P' + N_f}{2} \quad e^{4\Phi - 4\Phi_0} = \frac{2 \sinh(2\rho)^2}{(P^2 - Q^2)(P' + N_f)} \quad (24)$$

We require new IR asymptotes reflecting the addition of N_f sources. The ones befitting our case are [20]

$$P(\rho) = h_1 \rho + \frac{4N_f}{3} \left(-\rho \log \rho - \frac{1}{12} \rho \log(-\log \rho) + \mathcal{O} \left(\frac{\rho \log(-\log \rho)}{\log \rho} \right) \right) + \mathcal{O}(\rho^3 \log \rho) \quad (25)$$

Unfortunately, we have adopted an IR singularity caused by the high density stacking of the branes near $\rho = 0$ [10]. This leads to an unphysical background, which can also be seen through the study of the Wilson loops [25]

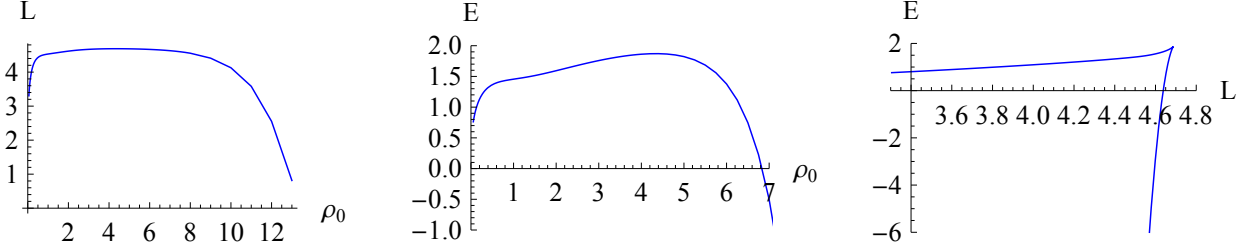


Figure 3: $\Phi_0 = 0$, $N_c = 1$, $N_f = 1$ and $h_1 = 4$

Note the cusp in the function $E(L)$. This is a visual indication of the fact that the way we introduced sources causes us problems.

With sight to the future analysis in this paper, it might be worth mentioning that the addition of sources has led our investigation into a regime where we can produce phase transitions on the physical (the lower) branch of the $E(L)$ plot:

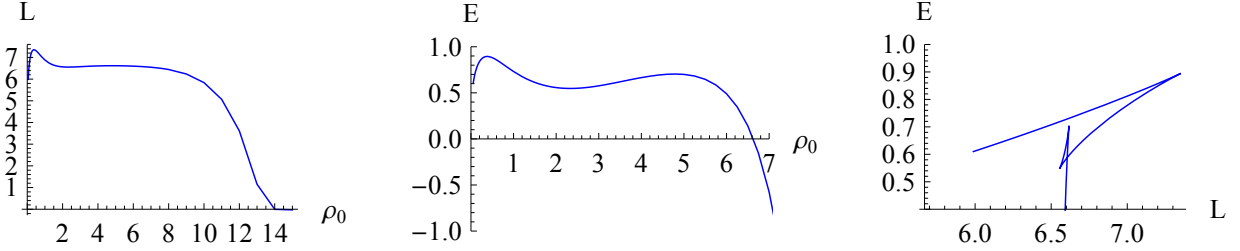


Figure 4: $\Phi_0 = 0$, $N_c = 5$, $N_f = 2$ and $h_1 = 29$

3.4 Sigmoid-like profiles

As described in [14], we can avoid this singularity by distributing the sources such that not all sources reach $\rho = 0$. Of importance is the fact that the density profile for the sources has a Maclaurin series with leading term at least of order $\mathcal{O}(\rho^3)$. A very nice and simple profile that fulfils the requirements - see [23] - is

$$S(\rho) = \tanh^4(2\rho) \quad (26)$$

which looks like

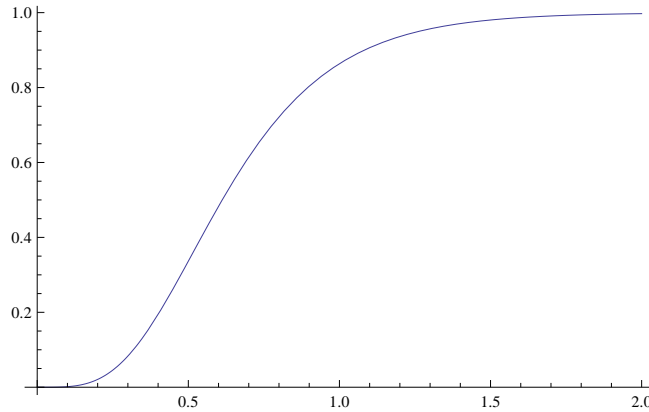


Figure 5: $S(\rho)$

Note that its IR expansion is

$$S(\rho) = 16\rho^4 - \frac{256}{3}\rho^6 + \frac{1536}{5}\rho^8 + \mathcal{O}[\rho^{10}] \quad (27)$$

as required. Following [14], we now have

$$(P'' + N_f S') + (P' + N_f S) \left[\frac{P' + Q' + 2N_f S}{P - Q} + \frac{P' - Q' + 2N_f S}{P + Q} - 4 \coth(2\rho) \right] = 0 \quad (28)$$

$$Q = \coth(2\rho) \left[\int_0^\rho dx \frac{2N_c - N_f S(x)}{\coth^2(2x)} \right]$$

$$e^{2k} = \frac{P' + N_f S}{2}$$

$$e^{4\Phi - 4\Phi_0} = \frac{2 \sinh(2\rho)^2}{(P^2 - Q^2)(P' + N_f S)}$$

Please note, comparing with the last subsection, it seems that the analysis was simply extended by replacing $N_f \rightarrow N_f S(\rho)$ everywhere. This is not quite true, seen for example at the new form the equation governing Q takes.

We get

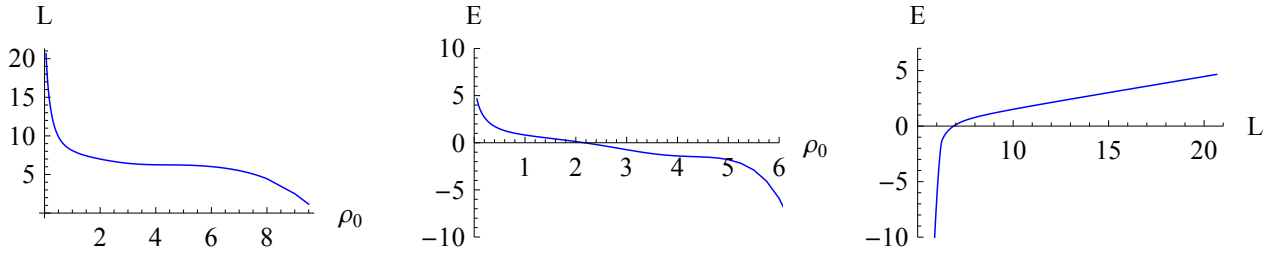


Figure 6: $\Phi_0 = 0$, $N_c = 5$, $N_f = 2$ and $h_1 = 11$

As one can see, $E(L)$ behaves smoothly again. Let us define h_{1c} to be the value of h_1 for which P remains linear in the UV. Note that $h_1 \approx h_{1c}$ here, thus P remains linear for quite some time, resulting in $L(\rho_0)$ plateauing before approaching 0.

3.5 Bump-like profiles

As argued in [1], the UV behaviour is improved by using a profile that decays like $e^{-\frac{4\rho}{3}}$. This is due to the fact that to preserve the KS like UV asymptotic behaviour, we need a profile that decays at least that fast. The presence of an exponentially increasing number of source branes, as is the case for a profile where $S \rightarrow 1$, behaves like the insertion of an irrelevant operator that deforms the UV dynamics. We also would not want a profile that decays faster to keep $T_{x_0 x_0}^{\text{sources}}$, representing the mass density of the sources, positive everywhere. To have $T_{x_0 x_0}^{\text{sources}} \rightarrow 0$ exactly, a profile that decays like $(\sinh(4\rho) - 4\rho)^{-1/3}$ is needed². Thus the following two profiles will be of importance. See [14, 23] for more details.

$$S(\rho) = \tanh^4(2\rho) e^{-\frac{4\rho}{3}} \quad (29)$$

$$\hat{S}(\rho) = \frac{\tanh^4(2\rho)}{(\sinh(4\rho) - 4\rho)^{1/3}} \quad (30)$$

²I thank Jerome Gaillard and Carlos Núñez for sharing that information prior to publication.

which look like

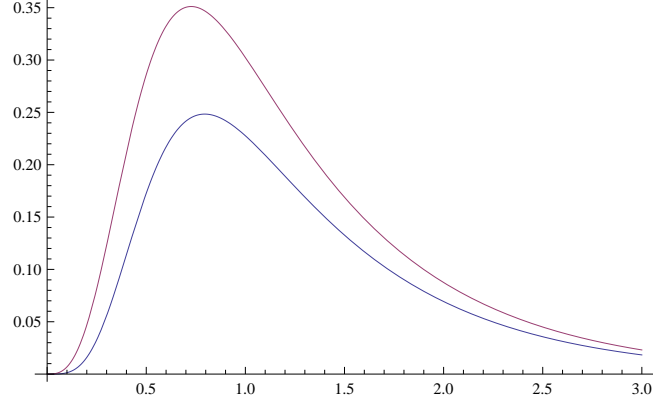


Figure 7: $S(\rho)$ is blue while $\hat{S}(\rho)$ is red

Note that $\hat{S}(0) = \frac{0}{0}$. While this can be quite easily analytically continued to be $\hat{S}(0) = 0$, numerical calculations using this profile have to be dealt with carefully. The approach in this paper is based on the following idea. As the IR expansion of this profile is

$$\hat{S}(\rho) = 6^{\frac{1}{3}}(4\rho^3 - \frac{112}{5}\rho^5 + \mathcal{O}[\rho^7]) \quad (31)$$

we define $\hat{S}(\rho) = a\rho^3 + b\rho^5$ for $0 < \rho < \epsilon$. We then solve for a and b by demanding that $\hat{S}(\rho)$ and $\hat{S}'(\rho)$ are continuous at ϵ . For simpler numerics at this stage, let us use $S(\rho)$ for now, and observe that we get a very similar picture to the previous subsections.

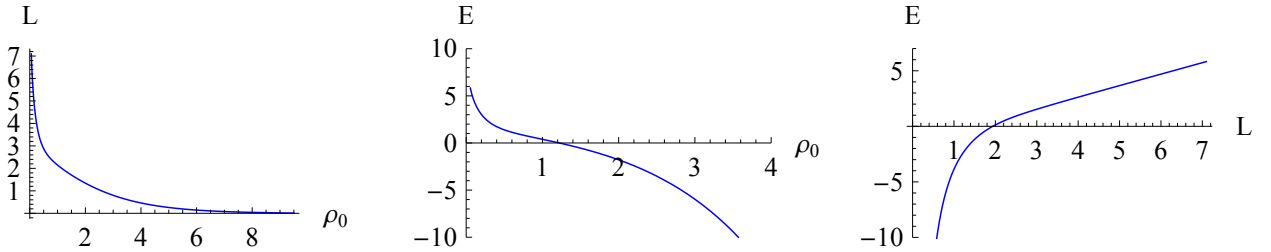


Figure 8: $\Phi_0 = 0$, $N_c = 1$, $N_f = 1$ and $h_1 = 3.12932$

4 Phase Transition

An interesting observable phenomenon that can be found is a phase transition. This was first observed for SQCD-like field theories in [27]. The interpretation of such a phenomena is similar to the phase transition of a boiling Van-der-Waals gas. Several other papers have found such a phenomena in similar cases since. See for example [13, 14, 25, 26, 31]

In order to find them for the theory discussed here, the parameter space of varying h_1 was explored. Please note that not all values of h_1 are valid. There always exists a critical value for h_1 , For which P grows linearly. For $h_1 > h_{1c}$, P grows exponentially in the UV and for $h_1 < h_{1c}$, P dies down to a singularity. Note the following figure.

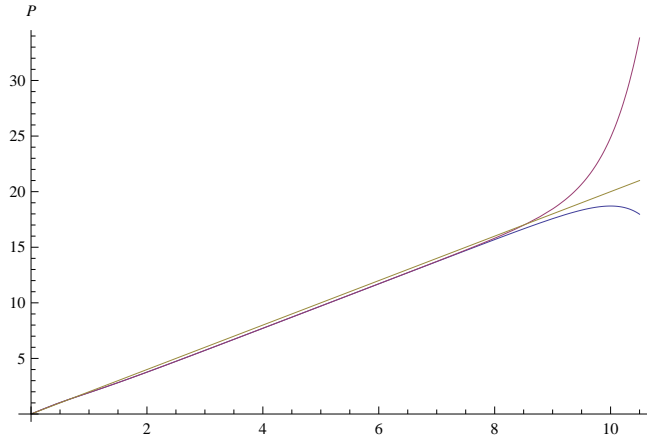


Figure 9: The green line represents P for h_{1c} , red $h_{1c} + \epsilon$ and blue $h_{1c} - \epsilon$

Our requirement for Φ to be bounded only allows exponentially growing solutions like the red curve. Thus a shooting procedure was used to find h_{1c} , which was used as starting value for our exploration into ever increasing values of h_1 . Unfortunately the search for a phase transition was unsuccessful for the three profiles (26), (29) and (30) mentioned above.

To see how to proceed from here, let us analyse that Van-der-Waals gas analogy from the beginning of the section more closely. Such a gas follows an equation of state of the form

$$P = \frac{NRT}{V - bN} - \frac{N^2a}{V^2} \quad (32)$$

where R, b, a are constants. Look at the diagrams borrowed from [13]

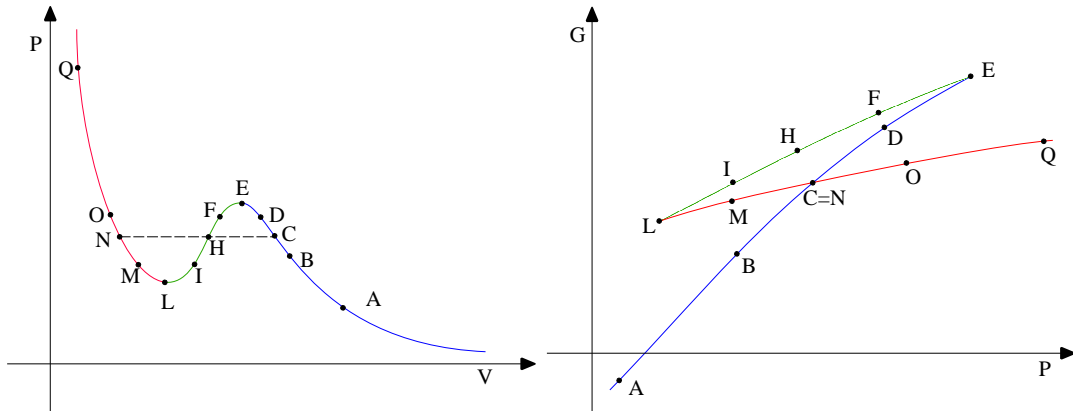


Figure 10: The pressure P as a function of the volume V (left panel) and the Gibbs free energy G as a function of the pressure P (right panel) for the same isotherm curve.

Clearly this analogy works by linking $L(\rho_0)$ to $P(V)$ as well as $E(L)$ to $G(P)$, such that $L \leftrightarrow P$, $\rho_0 \leftrightarrow V$ and $E \leftrightarrow G$. On the VdW side, it is clear that a phase transition will be observed, if $P(V)$ has a local maximum. This can be achieved by tuning two scales, dictated by the constants a and b , representing the interaction between the VdW gas particles and their non-zero size respectively. We have so far only explored a 1-dimensional parameter space. To increase our chances of success, we have to find another parameter to vary.

4.1 Introducing ρ_*

One thing one can try is to let the source branes not quite reach 0 but only start at some point ρ_* . This is easily achieved by multiplying the profile with a step function $\Theta(\rho - \rho_*)$

and performing the coordinate transformation $\rho \rightarrow \rho - \rho_*$. So, for example, our bump profile becomes $S(\rho) = \Theta(\rho - \rho_*) \tanh(2\rho - 2\rho_*)^4 e^{-4(\rho - \rho_*)/3}$.

Numerically, one can simply solve the unflavored system between 0 and ρ_* and then connect the system by using $P_{\text{unfl}}(\rho_*) = P(\rho_*)$ and $P'_{\text{unfl}}(\rho_*) = P'(\rho_*)$ as initial conditions for the flavored system. As shown in [14] this is justified if $S'(\rho_*) = S''(\rho_*) = 0$ which is true in our cases.

Here, a phase transition can be found regardless of which profile has been used. When we studied the parameter space in detail, we found that as we increased h_1 , $L(\rho_0)$ began to flatten in the region just below ρ_* until a peak appeared that kept getting more pronounced. See Figure 12. This behaviour was so typical that we conjecture that given any acceptable profile and $\rho_* > 0$ a phase transition can be found for this system. As an example look at the following figures.

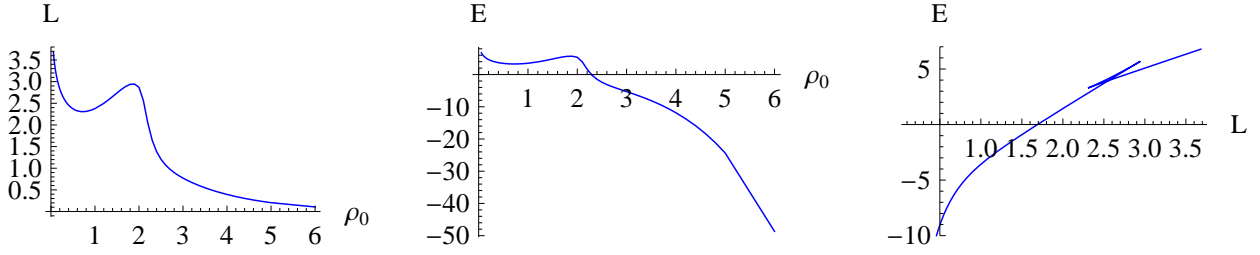


Figure 11: Here, $S(\rho) = \frac{\tanh^4(2(\rho - \rho_*))}{(\sinh(4(\rho - \rho_*)) - 4(\rho - \rho_*))^{1/3}}$, $\Phi_0 = 0$, $N_c = 1$, $N_f = 1$, $h_1 = 27$ and $\rho_* = 2$

The position of the phase transition is not random and has a nice physical interpretation. Before the phase transition the string explores only the sourcefull region, while afterwards a majority of the string is located in the sourceless region $\rho < \rho_*$. Thus the phase transition appears as more and more of the string enters the sourceless part.

For a given ρ_* , the value of h_1 that produces a phase transition is only bound below. This also has a nice physical picture associated to it. h_1 is directly related to $c+$, the expansion parameter of the UV asymptotes of P (20). $c+$ in turn is related to the scale at which P stops being linear and starts growing exponential. This in turn effects the gradient of $E(L)$ and thus the "speed" with which the string hits the sourceless region. For a more pictorial description, the reader may imagine a light ray getting refracted on a block of glass due to the fact that it is slowed down by the medium. The higher h_1 , the sooner P becomes exponential, and the "faster" the string hits the sourceless region. Above a certain threshold we observe phase transitions.

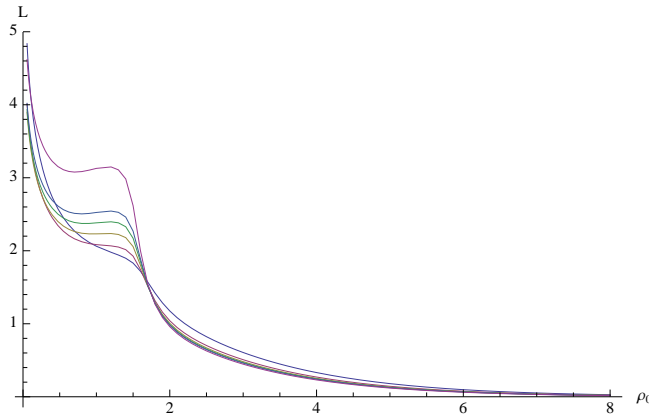


Figure 12: $L(\rho_0)$ for the exact same system for $h_1 = h_{1c} + 5$ at the bottom, till $h_1 = h_{1c} + 45$ in increments of 10 and then at the top for $h_1 = h_{1c} + 100$.

As the gradient of $L(\rho_0)$ grows to ∞ as $\rho_0 \rightarrow 0$, it is clear that the threshold for producing phase transitions, h_{1t} also grows to ∞ as $\rho_* \rightarrow 0$. This relationship between $\frac{dL(\rho_0)}{d\rho_0}$ and h_{1t} exists as h_1 represents how much $L(\rho_*)$ is lifted compared to close by points, and a steeper gradient requires more lift. See the figure above. For large ρ_0 , L is already quite flat, so even small values of h_1 will cause a bump to appear. For small ρ_0 , L is quite steep, so the initial increase in h_1 only flattens the profile. This is why we have not observed phase transitions just varying h_1 and effectively leaving $\rho_* = 0$.

4.2 Powers of tanh and x

Of course other variables do also have an effect on the Wilson loop and the associated phase transition.

For example, we can generalise the tanh component in the profiles discussed above from, $\tanh^4(2\rho)$ to $\tanh^{2n}(2\rho)$ where $n \geq 2$ is an integer. This has the conceptual imperfection though, that it pushes the flavour correction in the IR expansion of P to higher orders of ρ and thus effectively diminishes the effect of the flavour branes on the system more and more.

Also $x = \frac{N_f}{N_c}$ being a variable that affects many aspects of this system, also plays a role for how easy phase transitions can be found. As an example, here is $E(L)$ for systems equal to figure 11.

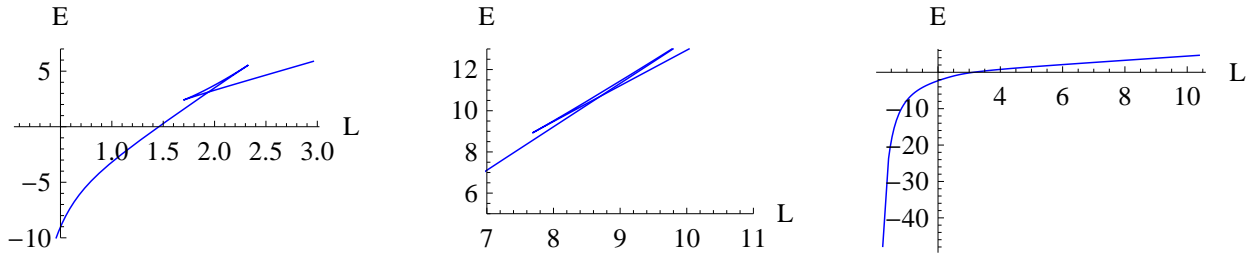


Figure 13: On the left $n = 5$, in the middle $x = 5$ and on the right $x = \frac{1}{5}$

Please note, that we can also find phase transitions for $x < 1$ but higher values of h_1 have to be used.

4.3 Different profiles

Again, one could simply take a whole other class of profiles. Very helpful was

$$S(\rho) = \begin{cases} 1 - \left(\frac{\cosh(4\rho q_1) + \cosh(4\rho q)}{2} - 1 \right) e^{-4\rho} & \text{if } \rho \geq 4 \\ \frac{2}{3} \frac{(\cosh(4\rho) - \cosh(4\rho q))^{\frac{3}{2}}}{(\cosh(4\rho q_1) - \cosh(4\rho q)) \sqrt{\cosh(4\rho) - 1}} & \text{if } \rho \leq \rho q_1 \\ \frac{2}{3} \frac{(\cosh(4\rho) - \cosh(4\rho q))^{\frac{3}{2}} - (\cosh(4\rho) - \cosh(4\rho q_1))^{\frac{3}{2}}}{(\cosh(4\rho q_1) - \cosh(4\rho q)) \sqrt{\cosh(4\rho) - 1}} & \text{otherwise} \end{cases}$$

based on the Flat Measure described in [14]. Here, analytical conditions are found, that the profile must fulfil, to produce desirable back reactions. These are then solved in a lengthy but logical procedure whose details are mentioned in the paper cited. If one wishes to have a decaying profile one could use $\hat{S}(\rho) = S(\rho)e^{-\frac{4}{3}\rho}$. These profiles have the following form

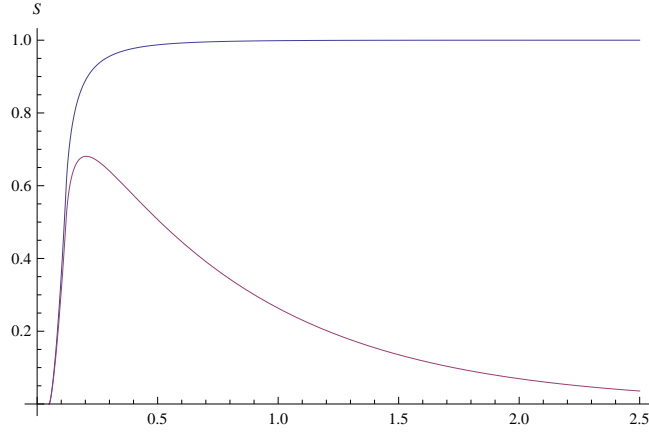


Figure 14: $S(\rho)$ is blue while $\hat{S}(\rho)$ is red

Both profiles lead to a phase transition. For $S(\rho)$ we have

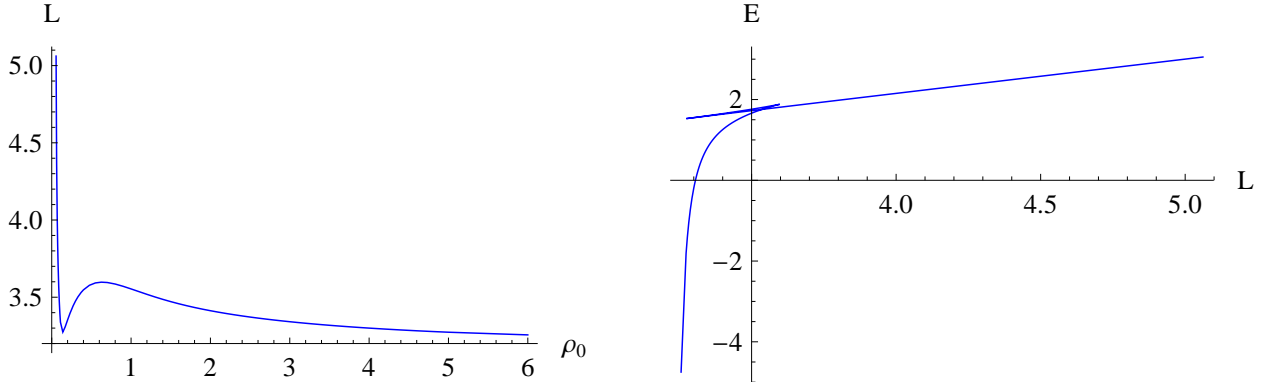


Figure 15: $N_c = N_f = 1$ and $h_1 = 3.9581$

And for $\hat{S}(\rho)$ we get:

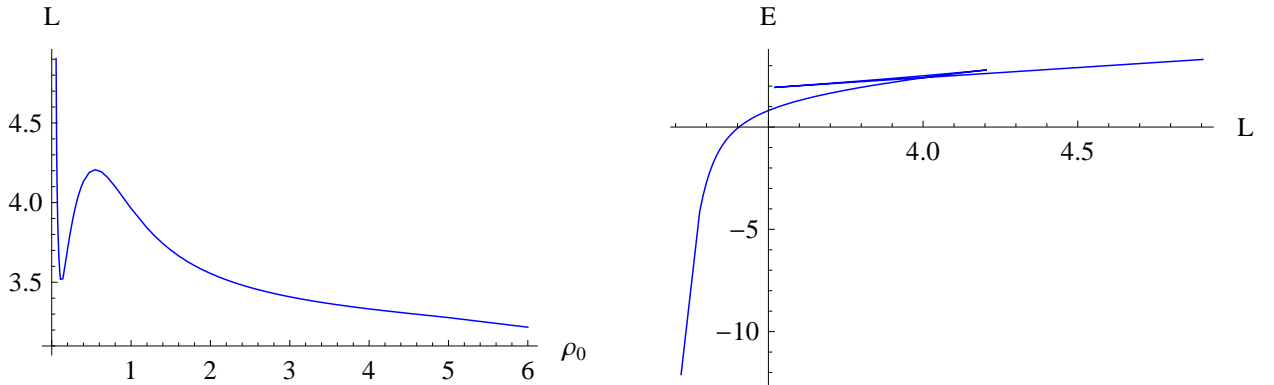


Figure 16: $N_c = N_f = 1$ and $h_1 = 3.25291$

ρq_1 is related to ρq via

$$\rho q_1 = \frac{1}{4} \text{arcosh}(\delta + \cosh(4\rho q)) \quad (33)$$

As δ decreases, the width of the brane distribution becomes smaller, The mass of the heaviest quark decreases and phase transitions are produced. Despite the large amount of control such

types of profiles offer, one should be aware, that their realization is not completely clean, in the sense that S' is not continuous everywhere, which can lead to problems as we will see in the following sections.

4.4 A curiosity

One quite surprising fact that was discovered during the search for phase transitions is that while most profiles require $h_1 \gg h_{1c}$ to show transition, profiles of the type $S(\rho) = \tanh^4(2(\rho - \rho_*))$ do not. For $h_1 \approx h_{1c}$, $P(\rho)$ will stay linear for quite some time before exhibiting exponential behaviour. This can be seen in Figure 9. In such cases, $L(\rho_0)$ will not immediately approach 0, but first approach a non-zero value α before, and β after the transition of P 's behaviour. Depending on several factors, such as the power of \tanh , we can force $\beta > \alpha$, leading to a very curious phase transition as shown in the following diagram.

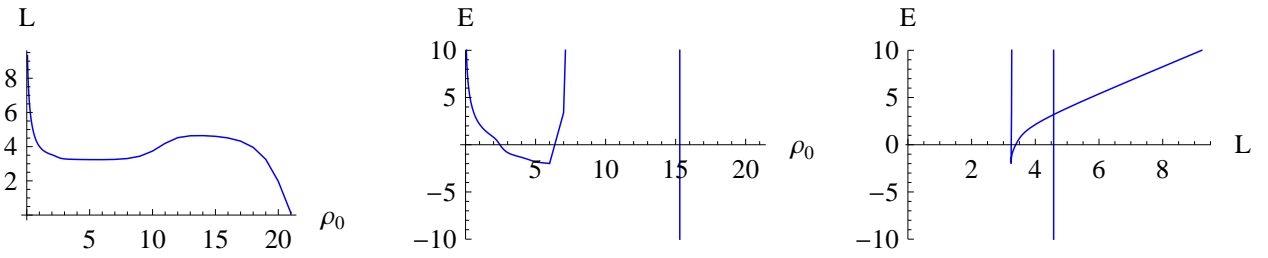


Figure 17: Here, $S(\rho) = \tanh^4(2(\rho - \rho_*))$, $N_c = N_f = 1$, $h_1 = \frac{1000519}{500000}$, $\rho_* = 2$

Please note that beside the phase transition the overall shape of $E(L)$ is equivalent to the expected, but one would have to plot it approximately between -10^7 and 10 to see it. Similarly $E(\rho_*)$ peaks at about 10^5 before descending rapidly.

In this section we have described several ways to achieve phase transitions. This can be best understood through the variation of two scales, dictated by h_1 , giving the "speed" of the increase of the potential with respect to separation length, and ρ_* , the scale at which the N_f sources kick in. However other techniques as well as influences of the system on the formation of phase transitions have been described. In particular, a general characteristic of profiles has been identified that is key in producing phase transitions. We need a region of high source density transitioning into a region of low density to be able to observe them. This appears to be a universal requirement. This obviously leaves the question, if this knowledge can be exploited to generalise the profile to describe new and interesting phenomena.

Also please note that while confinement has not been directly mentioned, it is generally understood that the theories discussed are confining. [15] gives several conditions for f and g that each guarantee confinement and it is straightforward to check that in all cases at least one of them is fulfilled.

5 Double phase transition

Something that has been missing so far in the literature, is the possibility to generalise this procedure, to find solutions with more than one phase transition. Below we list several types of profiles that allow us to generate these.

In this paper, we will restrict ourselves to profiles producing two phase transitions as proof of concept. In general though, these procedures seem to be able to produce an arbitrarily large amount of phase transitions if one so wishes.

5.1 Double Bump and Tumbling profiles

The first idea is to add several profiles of the form described in section 3.4 or 3.5. Here, we used

$$S(\rho) = \begin{cases} \tanh^4(2(\rho - \rho_{*1})) + \tanh^4(2(\rho - \rho_{*2})) & \text{if } \rho \geq \rho_{*2} \\ \tanh^4(2(\rho - \rho_{*1})) & \text{otherwise} \end{cases}$$

giving us a the following source profile.

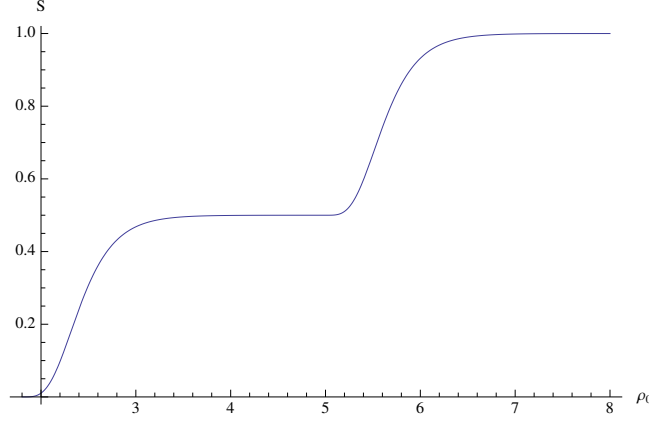


Figure 18: Here, $\rho_{*1} = 1.8$ and $\rho_{*2} = 5$

as well as

$$\hat{S}(\rho) = \begin{cases} \tanh^4(2(\rho - \rho_{*1}))e^{\frac{-4(\rho - \rho_{*1})}{3}} + \tanh^4(2(\rho - \rho_{*2}))e^{\frac{-4(\rho - \rho_{*2})}{3}} & \text{if } \rho \geq \rho_{*2} \\ \tanh^4(2(\rho - \rho_{*1}))e^{\frac{-4(\rho - \rho_{*1})}{3}} & \text{otherwise} \end{cases}$$

looking like

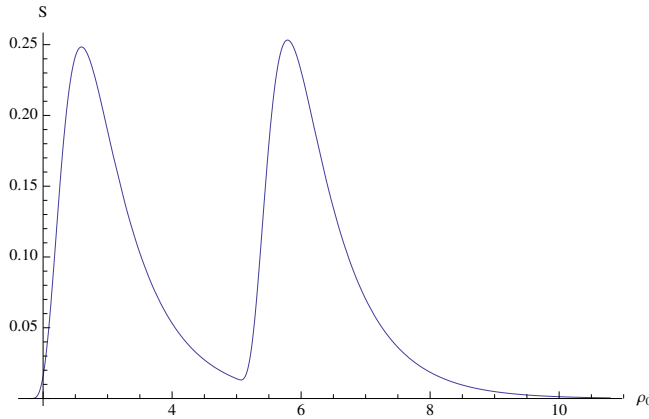


Figure 19: Here, $\rho_{*1} = 1.8$ and $\rho_{*2} = 5$

This leads to the following plots. For the Tumbling profile we have

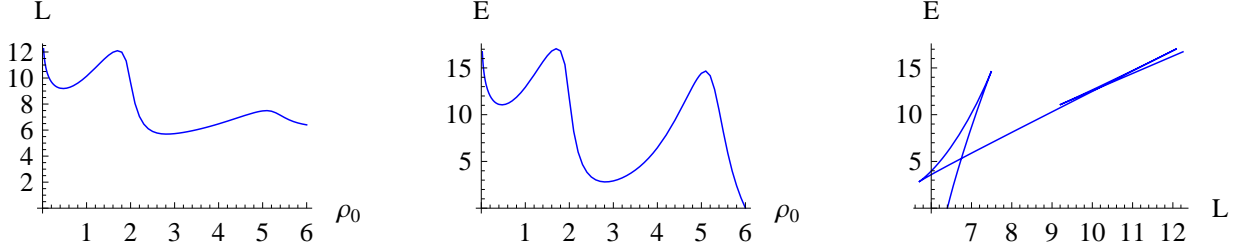


Figure 20: Here, $h_1 = 47$

And for the Double Bump:

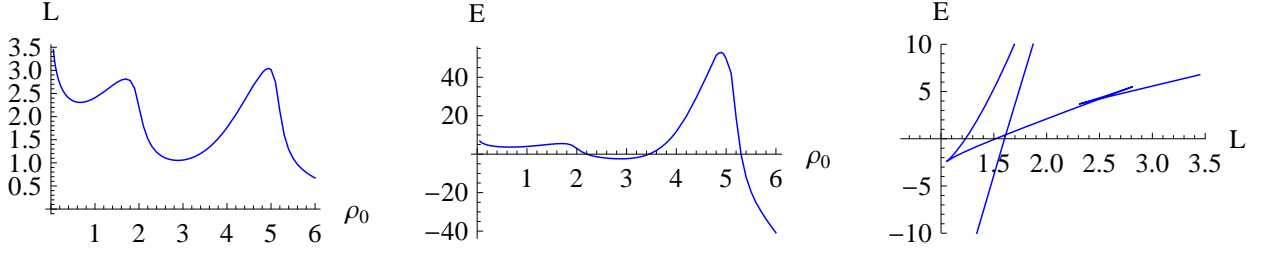


Figure 21: Here, $h_1 = 47$

Notice, that if the jump is from a region of high source density to a region with lower but non-zero source density, the smaller the difference, the harder it is to produce a phase transition, independent from the magnitude of the gradient of the jump. This can be seen in figure 20, where in the left-hand diagram the second peak is a lot less pronounced than in the right one.

Also this Tumbling profile in particular can be very interesting for Holographic Technicolor theories with Higgsing cascades. This case is discussed in [32].

Encouragingly, the central charge of the solutions of all profiles in this section, including plateau profiles are monotonically increasing and thus show no sign of unphysical behaviour. To calculate the central charge, we used the same definition as in [1]

$$c = \frac{\hat{h}^2 e^{2\Phi+2h+2g+4k}}{8(\partial_\rho \log[\sqrt{\hat{h}} e^{2\Phi+2h+2g+k}])^3} \quad (34)$$

This leads to graphs of the following shape:

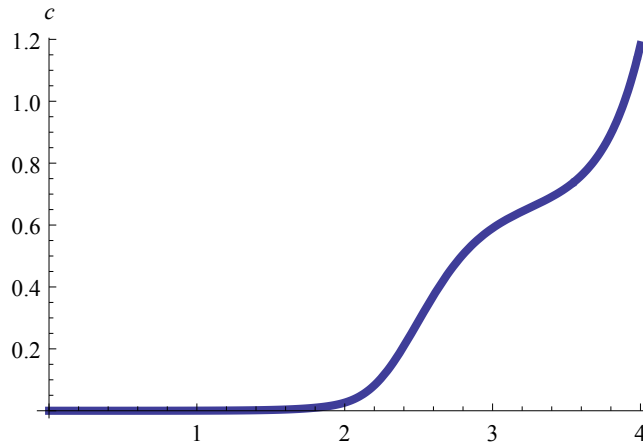


Figure 22: This is the central charge for the Tumbling case. For the other cases, the shape is similar, but c increases much faster

5.2 Plateau profiles

So far all the phase transitions observed come from the string moving from regions of high source density to regions of lower density. It would be interesting to see if this also works the other way around. Thus we would like to engineer profiles that quickly rise from 0 to 1, stay at 1 for some time before quickly decreasing back to 1. It is a major challenge to find such functions and so far none have been found that have a continuous first derivative. These can still be used, given that the discontinuity is well away from the regions of interest, such as the middle of the plateau, but will lead to an imperfection discussed below.

The easiest way to obtain profiles as described, is to use a profile that behaves like $S(\rho)$ from section 3.4 and 4.1 and then mirror it around the axis $\rho = c$, where $S(c) \approx 1$ and then forcing S to be 0 after it reached that value again. As an example we used

$$S(\rho) = \begin{cases} 0 & \text{if } \rho \geq \rho_* + 4 \\ \tanh^4(2(\rho - \rho_* - 4)) & \text{if } \rho_* + 4 \geq \rho \geq \rho_* + 2 \\ \tanh^4(2(\rho - \rho_*)) & \text{otherwise} \end{cases}$$

resulting in

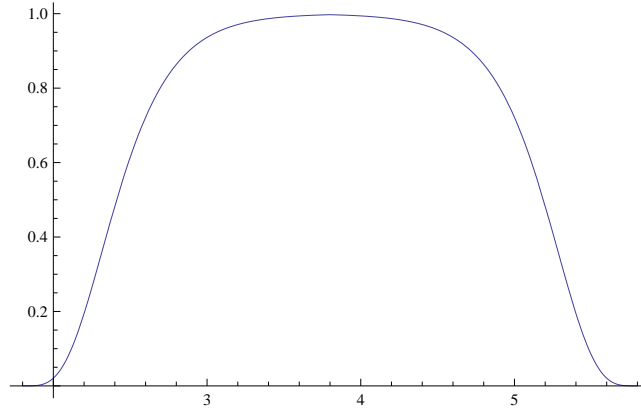


Figure 23: Here, $N_f = N_c = 1$, $\rho_* = 1.8$ and $h_1 = 47$

This leads to the following situation.

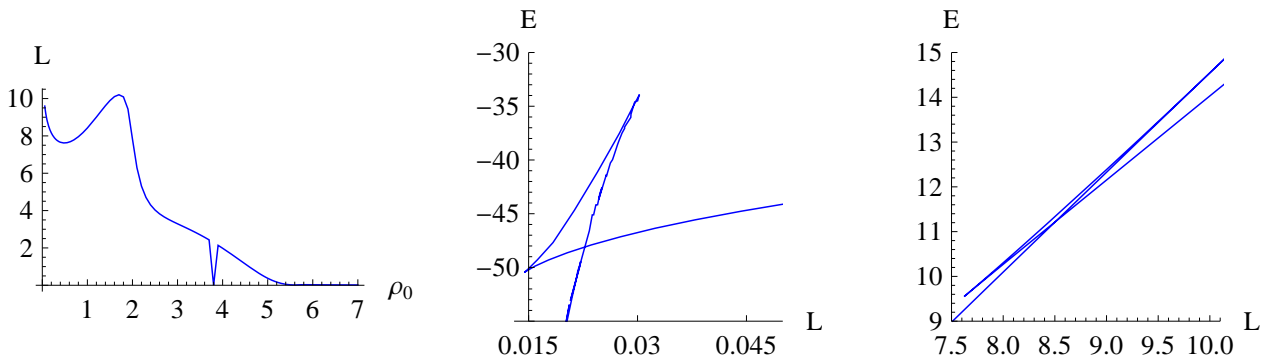


Figure 24: $L(\rho_0)$ and both physical phase transitions

Please note that $E(L)$ has 3 phase transitions, the two physical ones shown above, and one unphysical that is due to the discontinuity of S' at $\rho = 3.8$ at which the numerics produce the kink seen for $L(\rho_0)$. Note that the background does not contain any singularities per se. It is just at the exact point of the discontinuity that the numerics break down. Thus this discontinuity

is usually not noticeable and does not produce a third unphysical phase transition. In order to highlight this breakdown, $L(\rho_0)$ has been evaluated only at discrete points and then interpolated inbetween. Furthermore $L(\rho_0)$ was evaluated at exactly 3.8 to produce an erroneous data point. The purpose of this was to highlight the limitations of the numerical calculation, and illustrate the dangers of using profiles without a continuous derivative. Also due to the different scales and sizes at which the two phase transitions occur, we had to graph them separately to seem them clearly.

Thus we have strong evidence that phase transitions also occur when entering region of higher source density. This leads us to believe, that every bump profile actually produces two phase transitions per bump, that merge into another through an effect that is analogous to the effect that limits the angular resolution of lenses. Both bumps in $L(\rho_0)$ or $E(\rho_0)$ of, for example, figure 11 are so close together that they merge into one.

6 Conclusions

The basic idea of this paper was to study the details of Wilson loops of a novel class of solutions [1], that generalise the KS [16] and baryonic branch [24] solutions, that, by the addition of sources, move the QFT to the mesonic branch..

This was done constructively, by starting from a relatively plain wrapped branes model and slowly adding all the necessary features, keeping track of the properties of the Wilson loops of the theory at each stage.

Then, since a specific profile has not yet been obtained from a microscopic kappa-symmetric solution to the brane equations of motions, several profiles that feature desirable qualities have been examined.

Afterwards we discussed the possibility of creating a phase transition by tuning two scales dictated by h_1 and ρ_* . Also the effect of other variables of the theory on this phenomenon has been described. This construction of phase transitions has been very successful and yielded a positive outcome in every case. Furthermore, an interesting and so far unobserved phenomenon has been discovered and described.

Lastly, the possibility to create several phase transitions has been discussed, and several features a profile could have to produce these have been examined in detail, yielding a double phase transition in each case. In particular, a profile that might become useful for some extended holographic technicolor theories has been described.

My procedures should also be applicable to the 2+1 d equivalent that has been discussed in [26]

An interesting open question would be a detailed mathematical derivation of the exact requirements needed to obtain a phase transition. We may have some results on this in the near future.

Acknowledgments

I would like to thank several people for their support and guidance. Carlos Núñez, Daniel James Schofield, Niall Macpherson and Stephen Bennett all patiently helped me with all the questions that I could think of. Last but not least I thank Sebastian Halter for sharing some of his Mathematica code that has been very valuable.

My research is funded by the STFC.

References

- [1] E. Conde, J. Gaillard, C. Núñez and M. Piai, A. V. Ramallo [arXiv:1112.3350 [hep-th]]
- [2] J. M. Maldacena, Adv. Theor. Math. Phys. **2**, 231 (1998) [Int. J. Theor. Phys. **38**, 1113 (1999)] [hep-th/9711200].
- [3] S. S. Gubser, I. R. Klebanov, A. M. Polyakov, Phys. Lett. **B428**, 105-114 (1998). [hep-th/9802109].
- [4] K. G. Wilson, Phys. Rev. D **10**, 2445 (1974).
- [5] S. J. Rey and J. T. Yee, Eur. Phys. J. C **22**, 379 (2001) [arXiv:hep-th/9803001].
- [6] S. A. Hartnoll, S. P. Kumar JHEP 0608:026,2006 [arXiv:hep-th/0605027] N. Drukker, B. Fiol JHEP0502:010,2005 arXiv:hep-th/0501109
- [7] J. M. Maldacena, Phys. Rev. Lett. **80**, 4859 (1998) [arXiv:hep-th/9803002].
- [8] J. Maldacena and D. Martelli, JHEP **1001**, 104 (2010) [arXiv:0906.0591 [hep-th]].
- [9] R. Casero, C. Nunez, A. Paredes, Phys. Rev. **D73**, 086005 (2006). [hep-th/0602027].
- [10] C. Nunez, A. Paredes and A. V. Ramallo, Adv. High Energy Phys. **2010**, 196714 (2010) [arXiv:1002.1088 [hep-th]].
- [11] E. Witten, Adv. Theor. Math. Phys. **2**, 505 (1998) [hep-th/9803131].
- [12] J. M. Maldacena and C. Nunez, Phys. Rev. Lett. **86**, 588 (2001). [arXiv:hep-th/0008001].
- [13] C. Nunez, M. Piai and A. Rago, Phys. Rev. D **81**, 086001 (2010) [arXiv:0909.0748 [hep-th]]
- [14] E. Conde, J. Gaillard and A. V. Ramallo, JHEP **1110**, 023 (2011) [arXiv:1107.3803 [hep-th]].
- [15] J. Sonnenschein, arXiv:hep-th/0003032.
- [16] I. R. Klebanov and M. J. Strassler, JHEP **0008**, 052 (2000) [arXiv:hep-th/0007191].
- [17] C. Hoyos-Badajoz, C. Nunez, I. Papadimitriou, Phys. Rev. **D78**, 086005 (2008). [arXiv:0807.3039 [hep-th]].
- [18] R. Casero, C. Nunez, A. Paredes, Phys. Rev. **D77**, 046003 (2008). [arXiv:0709.3421 [hep-th]].
- [19] D. Elander, J. Gaillard, C. Nunez, M. Piai, JHEP **1107**, 056 (2011). [arXiv:1104.3963 [hep-th]].
- [20] J. Gaillard, D. Martelli, C. Nunez and I. Papadimitriou, Nucl. Phys. B **843**, 1 (2011) [arXiv:1004.4638 [hep-th]]. E. Caceres, C. Nunez, L. A. Pando-Zayas, JHEP **1103**, 054 (2011). [arXiv:1101.4123 [hep-th]].
- [21] L. Martucci, P. Smyth, JHEP **0511**, 048 (2005). [hep-th/0507099].
- [22] F. Bigazzi, R. Casero, A. L. Cotrone, E. Kiritsis, A. Paredes, JHEP **0510**, 012 (2005). [hep-th/0505140].
- [23] A. Barranco, E. Pallante, J. G. Russo, JHEP **1109**, 086 (2011). [arXiv:1107.4002 [hep-th]].

- [24] A. Butti, M. Grana, R. Minasian, M. Petrini and A. Zaffaroni, JHEP **0503**, 069 (2005) [arXiv:hep-th/0412187].
- [25] S. Bennett, Annals Phys. **326**, 2934-2956 (2011). [arXiv:1102.5731 [hep-th]].
- [26] N. Macpherson JHEP06(2012)136 [arXiv:1204.4222 [hep-th]]
- [27] F. Bigazzi, A. L. Cotrone, C. Nunez and A. Paredes, Phys. Rev. D **78**, 114012 (2008) [arXiv:0806.1741 [hep-th]].
- [28] A. Dymarsky, I. R. Klebanov, N. Seiberg, JHEP **0601**, 155 (2006). [hep-th/0511254].
- [29] C. Krishnan, S. Kuperstein JHEP 0805:072,2008 [arXiv:0802.3674 [hep-th]].
- [30] C. Núñez, I. Papadimitriou, M. Piai Int.J.Mod.Phys.A25:2837-2865,2010 arXiv:0812.3655 [hep-th].
- [31] C. Bigazzi, A. L. Cotrone, A. Paredes, A. Ramallo Fortsch.Phys.57:514-520,2009 arXiv:0810.5220 [hep-th].
- [32] E. Conde, J. Gaillard, C. Nunez, M. Piai and A. V. Ramallo, Phys. Lett. B, Volume 709, Issues 4-5, March 2012, 385 arXiv:1112.3346 [hep-th].